Comparison of Aerodynamic Performances of Various Airfoils from Different Airfoil Families Using CFD

Article *in* Wind and Structures · March 2021

DOI: 10.12989/was.2021.32.3.239

3 authors, including:

Mehmet Numan Kaya
Necmettin Erbakan Üniversitesi
19 PUBLICATIONS **157** CITATIONS

SEE PROFILE

Huseyin Kurt
Necmettin Erbakan Üniversitesi
69 PUBLICATIONS **1,111** CITATIONS

SEE PROFILE

Comparison of Aerodynamic Performances of Various Airfoils from Different Airfoil Families Using CFD

Mehmet Numan Kaya*[1], Ali Rıza Kök[1] and Hüseyin Kurt[1]

[1]Department of Mechanical Engineering, Necmettin Erbakan University, Konya, Turkey

Abstract. In this study, three airfoil families, NACA, FX and S, in each case three from each series with different shapes were investigated at different angles of attack using Computational Fluid Dynamics (CFD) method. To verify the CFD model, simulation results of the NACA 0012 airfoil was compared against the available experimental data and k-ω SST was used as the turbulence model. Lift coefficients, lift to drag ratios and pressure distributions around airfoils were obtained from the CFD simulations and compared each other. The simulations were performed at three Reynolds numbers, $Re=2\times10^5$, 1×10^6 and 2×10^6, and angle of attack was varied between -6 and 12 degrees. According to the results, similar lift coefficient values were obtained for symmetric airfoils reaching their maximum values at similar angles of attack. Maximum lift coefficients were obtained for FX 60-157 and S 4110 airfoils having lift coefficient values around 1.5 at $Re=1x10^6$ and 12 degrees of angle of attack. Flow separation occurred close to the leading edge of some airfoils at higher angles of attack, while some other airfoils were more successful in keeping the flow attached on the surface.

Keywords: aerodynamics; airfoil; CFD; NACA series; FX series; S series

1. Introduction

Airfoils have an important role in aerodynamic applications because the performance of a body is influenced by the aerodynamic shape (Tarhan and Yilmaz 2019, Alonso-Estebanez *et al.* 2018). Airfoils are being used in a wide variety of areas, e.g. wind turbine blades, axial compressor and fan blades, propellers, wings. Before designing a complete body including airfoils, it is crucial to design or select the proper airfoil according to the application area. Therefore, a lot of studies have been performed to improve efficiencies of dynamic bodies by using airfoils and lots of airfoil shapes have been investigated concerning their performances (Tasci *et al.* 2020, Basta *et al.* 2020). Flow over the NREL S826 airfoil at low Reynolds numbers has been investigated by Cakmakcioglu *et al.* (2014) using CFD and authors found that the results are in fair agreement with available experimental data. Similarly, Patel *et al.* (2014) have studied the flow around the NACA 0012 airfoil

*Corresponding author, Ph.D., E-mail: mnkaya@erbakan.edu.tr

using CFD and concluded that numerical simulation results show close agreement with experimentally obtained results. Sreejith and Sathyabhama (2018) have investigated the effect of boundary layer trips on aerodynamic performance of E216 airfoil. According to the results of the study, boundary layer trips improve the aerodynamic performance of the airfoil by eliminating laminar separation bubbles partially or completely. Siauw *et al.* (2010) have performed a study on dynamics of attachment and separation over the NACA 0015 airfoil by using a fluid vortex generator and analyzing the flow of the near wake via conditional PIV measurements. They have found out that the process of attachment shows a strong transient effect linked with the passage of a starting vortex. Aranake *et al.* (2015) have carried out numerical simulations of S809 airfoil to calculate the lift coefficients for different angles of attack. Authors have compared the results with the NREL experimental data and those were in a good agreement. Troolin *et al*. (2006) have added a gurney flap to the NACA 0015 airfoil and investigated the performance of the new design numerically. They concluded that adding gurney flap was useful because an increase in lift coefficient was obtained while drag coefficient was not changed. Li *et al.* (2020) performed a study on airfoil design for wind turbines located in low rated wind speed regions and indicated that the framework proposed in the study is able to design different airfoils suited for site-specific blade requirements. Younsi *et al*. (2019) have studied the aerodynamics of an elliptic airfoil that is subjected to translation and rotation motion considering the effect of the ground and found out that the most of the lift production is due to the delayed stall associated with the leading-edge vortex mechanisms and rapid pitching. Bhat *et. al.* (2013) investigated oscillating NACA 0012 airfoils at low Reynolds Numbers around the stall angle and concluded that leading edge vortex is formed due to shear layer separation from the leading edge. Matyushenko *et al*. (2017) studied flow around various airfoils with different shapes and thicknesses using two-dimensional RANS. They have found out that the computational results and the experimental data are in a good agreement at small angles of attack (up to 7-12°) and at higher angles of attack the lift coefficient exceeds the experimental value. Abinav *et al.* (2016) analyzed a Co Flow Jet (CFJ) airfoil using CFD and claimed that the stall margin is improved by 33% to 67% compared to the baseline airfoil using CFJ airfoils. Rostami *et al.* (2011) investigated NACA0012 airfoil considering unsteady and incompressible turbulent flows around stationary and flapping airfoil. According to the results obtained by examining using different turbulence models, it is found that nonlinear models predict smaller stall angle compared with the linear ones. Authors have also added that the effect of reduced frequency is significant. Anitha *et al.* [(2018) have studied on optimization of NACA4412 airfoil shape using genetic algorithm and particle swarm optimization methods and compared the baseline and optimized airfoils concluding that better aerodynamic performance can be obtained by shape optimization of airfoils. Similarly, Spurthy *et al.* (2016) have investigated the effects of surface modifications on aerodynamic characteristics of an airfoil and found aerodynamic efficiency can be increased by modifications. Using same airfoil, Kapsalis *et al.* (2016) have compared the effect of three transition models on the CFD predictions and concluded that the results obtained by using the K–V transition model are in better agreement with available experimental data. Morgado *et al.* (2016) compared CFD and XFOIL performance predictions for high lift low Reynolds number airfoils and found out that XFOIL results are as good as CFD results. Li *et al.* (2020) developed a new airfoil shape by using optimization algorithms and optimized it with control of the discretization error. Moreover, the accuracy of the optimized airfoil shape was investigated by the authors. Eggert and Rumsey (2017) performed a CFD study of NACA 0018 airfoil with flow control using two different Reynolds-Averaged Navier-Stokes codes used in two-dimensional computations along with several different turbulence models and concluded that and Shear Stress Transport (SST) and Spalart-Allmaras (SA) turbulence models produced

reasonable results. Srinath *et al.* (2009) studied the flow over NACA 0012 airfoil at angle of attack 4 and 12 for Re≤500. Tests were carried out with different functions. Based on his solutions he found out that there is sensitiveness on the flow in accordance with Reynolds number. Bansal *et al.* (2017) analyzed an airfoil in uniform flow under different angles of attack. The results have shown that a CFD modelling can be effectively used for airfoil design thanks to acceptable solutions compared to experiments. In this study, the flow around various symmetric and asymmetric airfoils from three airfoil families were investigated to find out the aerodynamic similarities and differences between these. Zamani *et al.* (2016) investigated the airfoil thickness effects on the performance of J-shaped straight blade vertical axis wind turbine and found out that opting for the higher thickness in J-shaped profiles for the blade sections have a great effect on the performance. Lin and Chiu (2020) investigated the influence of leading edge protuberances using FX63 airfoil and found increments at the power performance when equipped with protuberances. They have concluded that the average power output was increasing and more stabilized. In this study, the flow around various symmetric and asymmetric airfoils from three airfoil families were investigated to find out the aerodynamic similarities, differences and effect of the shape on aerodynamic parameters. The relationship between the aerodynamic shape and lift, drag and pressure distributions are examined in detail to find out the effect of each parameter to other. Lift coefficients and lift to drag ratios were compared in each group and shown in comparison to the other group. This study will be helpful to select an airfoil according to the airfoils aerodynamic shape, pressure and velocity distributions, lift and drag values. In addition, the current work will contribute to better understanding of aerodynamic effects according to the shape and assist researchers especially when designing or selecting an airfoil.

2. Material and Method

A body inside of air is always under aerodynamic forces and these forces are known as lift, drag, thrust and weight (Ilhan *et al.* 2018, Elsakka *et al.* 2018, Manwell *et al.* 2010, Kose and Kaya 2018). These forces are easily influenced by the shape of the body and air motion (Celik *et al.* 2020). An airfoil is the cross-sectional shape of a blade or wing which are used in various application areas. Airfoils are generally designed to create less pressure above the wing to create lift. Lift is usually presented as dimensionless number which is called lift coefficient and which can be calculated for airfoils using the Eq. 1. In Eq. 1, F_L is the lift force (N), ρ is the density (kg/m^3), V is the wind speed (m/s), A is the swept area (m^2) and c is the chord length (m). Similarly, drag coefficient can be calculated using Eq. 2 where F_D stands for the drag force (N). Pressure coefficient can be calculated using Eq. 3 where ΔP in stands for the pressure difference (Pa) (Manwell *et al.* 2010).

$$C_L = \frac{F_L}{0.5\rho V^2 c} \tag{1}$$

$$C_D = \frac{F_D}{0.5\rho V^2 c} \tag{2}$$

$$C_p = \frac{\Delta P}{0.5\rho V^2} \tag{3}$$

There are some base terms which are important to describe the shape of the airfoil and understand the forces on an airfoil. The chord is the connection line between leading and trailing edge. The

camber line is the line which is exactly in the middle of upper and lower surfaces and is generally above the chord line for a cambered airfoil. The trailing edge is the rear point of an airfoil where the maximum curvature is located. The leading edge is the front point of an airfoil where maximum curvature forms. Maximum thickness is the maximum distance between the bottom edge to the top edge and the angle between the chord line and the airflow is defined as angle of attack (AoA) (Manwell *et al.* 2010).

2.1 CFD Method

Computational Fluid Dynamics (CFD) is widely used in a range of applications where the main focus is flow. In this study, CFD method is used to simulate the flow around the airfoils. The governing equations of CFD are conservation of mass, momentum and energy. Navier-Stokes equation is a vector equation obtained by using Newton's Law of Motion to a fluid element and is also called the momentum equations. It is supplemented by the mass conservation equation that is also called continuity equation (ANSYS 2017) Conservation of mass and momentum equations are given in Eq. 4 and Eq. 5 respectively (Tu *et al.* 2018). In Eq. 4, $\vec{V}$ is velocity vector which is function of time (t) and location (x,y,z) and which has local velocity components (u,v,w), S_M is the source term. In Eq. 5, p is static pressure, $\bar{\bar{r}}$ is stress tensor, $\rho\vec{g}$ and $\vec{F}$ are gravitational body force and external body force respectively. The Equation for the Stress tensor $\bar{\bar{r}}$ is given in Eq. 6 where μ is the viscosity, I is the unit tensor (ANSYS, 2017, Tu *et al.* 2018).

$$\frac{\partial \rho}{\partial t} + \nabla \cdot \left(\rho \vec{V}\right) = S_M \tag{4}$$

$$\frac{\partial}{\partial t}\left(\rho \vec{V}\right) + \nabla \cdot \left(\rho \vec{V}\vec{V}\right) = -\nabla p + \nabla \cdot (\bar{\bar{r}}) + \rho\vec{g} + \vec{F} \tag{5}$$

$$\bar{\bar{r}} = \mu\left[\left(\nabla \vec{V} + \nabla \vec{V}^T\right) - \frac{2}{3}\nabla \vec{V} I\right] \tag{6}$$

As the turbulence model k-ω Shear Stress Transport (SST) was selected because it is successful in near wall regions. The k-ω SST turbulence model is developed by Menter (1994). The SST formulation was devised to effectively blend the free-stream correct behavior of the k - ε turbulence closure with the robust and accurate formulation of the k-ω model in the near wall region (Argyropoulos and Markatos 2015). Menter (1992) mentioned that inclusion of transport effects into the formulation of the eddy-viscosity has provided the ability to completely predict flow separation and adverse pressure gradient. The k-ω SST model is using two equations, turbulent kinetic energy (k) and length scale (ω), for solving numerical problems (Gresho 1991, Menter 1992). The equations of turbulence kinetic energy and specific dissipation rate are given in Eq. 7 and 8, respectively.

$$\frac{\partial(\rho k)}{\partial t}+\frac{\partial(\rho u_i k)}{\partial x_i}=\frac{\partial}{\partial x_j}\left[(\mu+\sigma_k\mu_t)\frac{\partial k}{\partial x_j}\right]+\tau_{ij}\frac{\partial u_i}{\partial x_j}-\beta^*\rho\omega k \tag{7}$$

$$\frac{\partial(\rho\omega)}{\partial t}+\frac{\partial(\rho u_i \omega)}{\partial x_i}=\frac{\partial}{\partial x_j}\left[(\mu+\sigma_\omega\mu_t)\frac{\partial \omega}{\partial x_j}\right]+\frac{\gamma}{v_t}\tau_{ij}\frac{\partial u_i}{\partial x_j}-\beta^*\rho\omega^2+2\rho\,(1-F_1)\sigma_{\omega 2}\frac{1}{\omega}\frac{\partial k}{\partial x_j}\frac{\partial \omega}{\partial x_j} \tag{8}$$

The first and second terms on the left part of the Eq. 7 are transient and convection terms for turbulent kinetic energy k, respectively. On the right side of the equation is the diffusion, production and dissipation terms, respectively. In Eq. 8, first three terms on the right and two terms on the left are the terms for turbulent frequency. In addition, the cross-diffusion term, source term, has been included in the equation which is the transition term from ε to ω. Default model constants are used in ANSYS-Fluent 18.0 (ANSYS 2017). As the turbulence specification method, turbulence intensity and viscosity ratio were used in this study having the values of 0.1 to 10, respectively and as the scheme method coupled was used.

2.2 Flow domain and grid generation

The flow domain consists of a semicircle with a radius of 25 m and a rectangular domain with a length of 65 m. The airfoil is located at the semicircular center. As shown in Fig. 1, boundary conditions were set as velocity inlet and pressure outlet at the inlet and outlet, and the airfoil is defined as no slip wall. The inlet velocities were calculated according to the Reynolds number. The pressure and the temperature were assumed to be 1 atm and 15 °C, respectively. At this temperature, the atmospheric pressure is 101325 Pa, the density of the air is ρ=1.225 kg/m^3, and the dynamic viscosity is μ=1.7894×10^{-5} kg/ms.

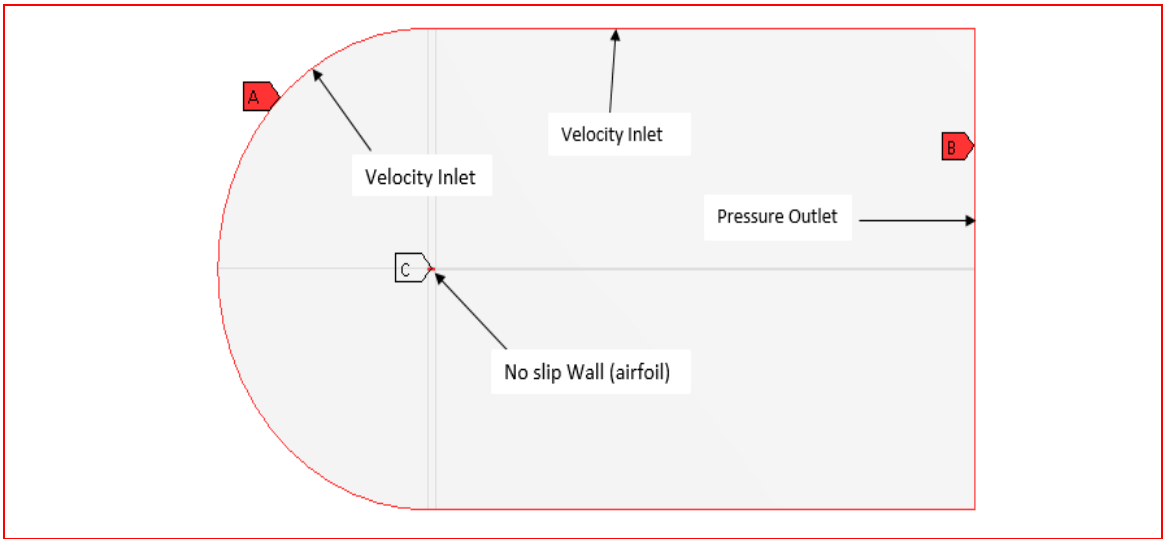

Fig. 1 Boundary conditions

The flow domain was divided into six parts to create a structured grid. By defining edge sizing, a very intense mesh was created around the airfoil which is the region of interest. For an accurate comparison, all airfoils are meshed using the same sizing functions and methods. To accurately solve the flow around the airfoil, the wall y+ is kept under 1 which is necessary for the used turbulence model. Finally, a grid containing around 300000 mesh elements were created. Pictures from the grid are presented in Fig. 2.

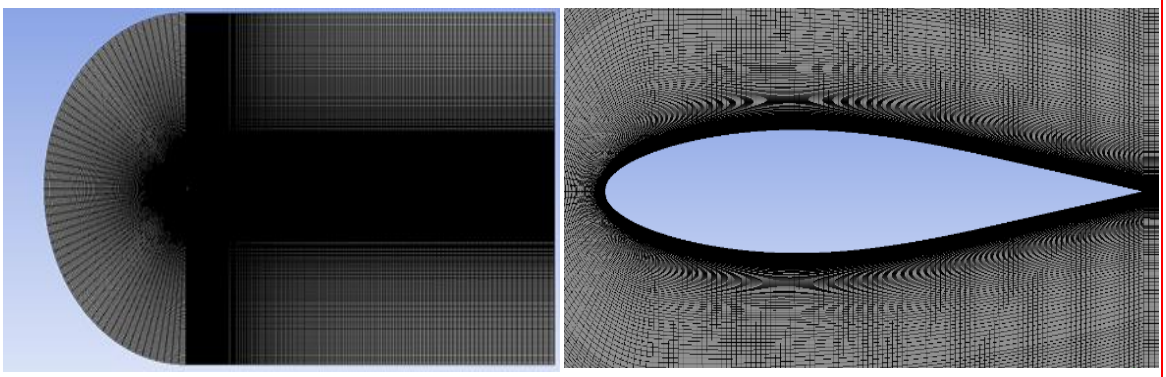

Fig. 2 Grid model

2.3 Verification of the CFD model

In order to verify the accuracy of the CFD model, the lift and the lift-to-drag ratio curves were compared at Reynolds number 1×10^6 with the available experimental data (Abbott and Doenhoff 1959). In Fig. 3, experimental lift coefficients were compared with the ones obtained from CFD simulations and lift-to-drags were compared in Fig. 4. The lift coefficients are in a very good agreement between angles of attack from -4° to 4 degree and after angle of attack of 4°, results are in a good agreement but the experimental lift coefficients are slightly higher than the CFD results. The lift-to-drag ratio curves are generally in agreement however under zero degrees of angle attack experimental values are lower than the CFD ones while after zero degrees CFD values are lower than experimental ones.

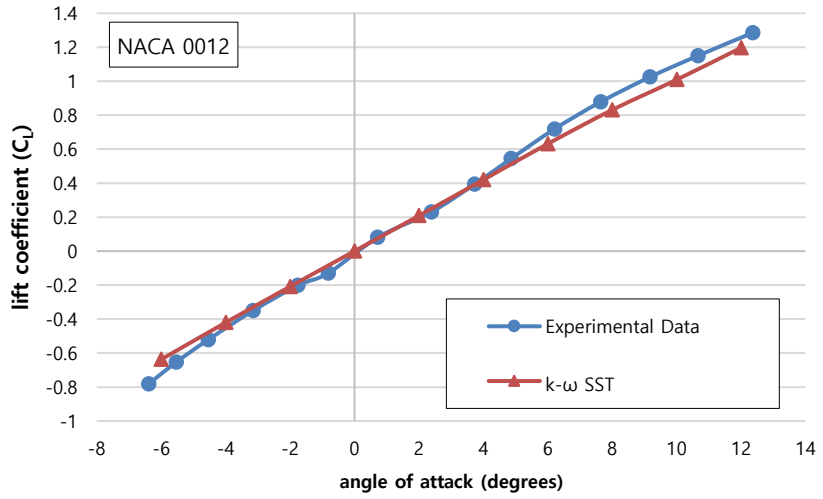

Fig. 3 Comparison of lift coefficients obtained from CFD simulations with the available experimental data

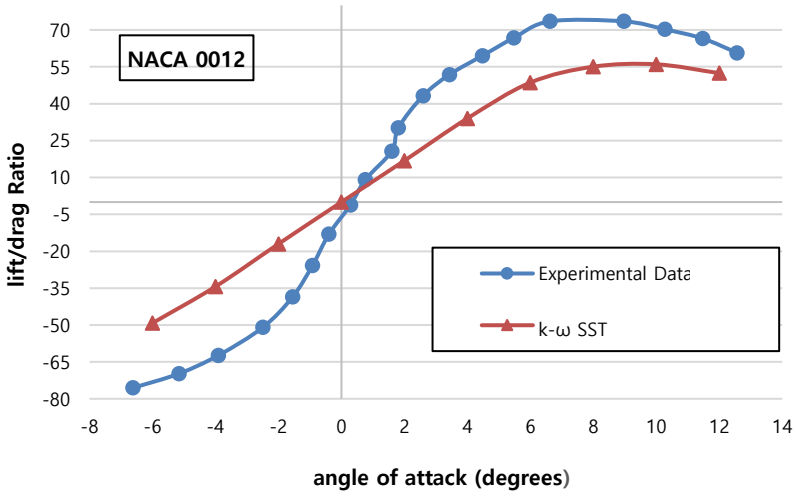

Fig. 4 Comparison of lift-to-drag ratios obtained from CFD simulations with the available experimental data

2.4 Airfoils studied

In this study, nine airfoils from three airfoil families, NACA, FX and S, in each case three from each series with different shapes were investigated. These are FX 60-157, FX 68-120, FX 71-120, NACA 0012, NACA 63-015A, NACA 6409, S 806, S 1012 and S410. Among those, four airfoils, FX 71-120, NACA 0012, NACA 63-015A and S 1012, are symmetrical airfoils. The studied airfoil shapes are presented in Fig 5.

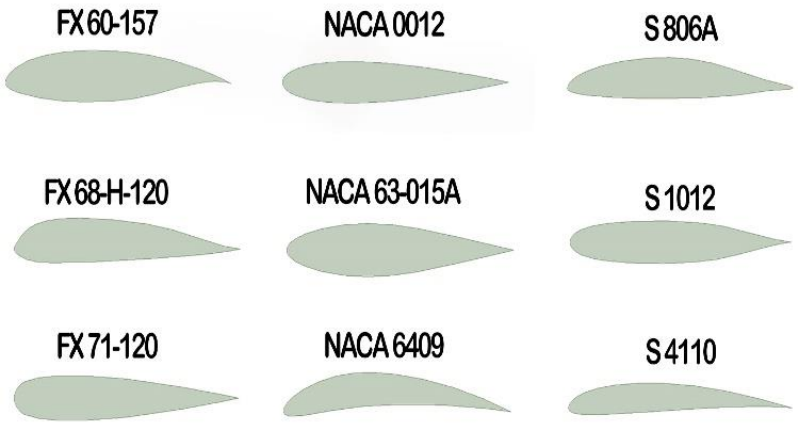

Fig. 5 Airfoils studied: FX series (left), NACA series (middle) and S series (right)

3. Results and Discussions

In this work, various airfoils from FX, NACA and S airfoil families were investigated at different angle attacks. According to the results it is clear that with increasing Reynolds number, the lift coefficients are increasing. Similar results were obtained for similar shaped airfoils as expected. Highest lift coefficient was obtained for the FX 60-157 with the value of 1.5512 at $Re = 2 \times 10^6$. At $Re = 2 \times 10^5$, stall was occurred for FX 71-120 airfoil between 10-12°. Lift coefficients and lift-to-drag ratios for NACA 0012, NACA 63-015A and NACA 6409 are presented in Fig. 6. Comparing the lift coefficients of the NACA airfoils, it is clear that NACA 63-015A has the worst aerodynamic performance. Highest lift coefficients were obtained for the NACA 6409 at all three Reynolds numbers having values nearly values of 1.18, 1.58 and 1.59 at $Re = 2 \times 10^5$, 1×10^6 and $Re = 2 \times 10^6$, respectively at 12 degrees angle of attack. NACA 0012 and NACA 63-015A have less lift coefficient values around 1.0-1.2 and 0.8-1.0, respectively. Lift/drag ratios of NACA 0012 and NACA 63-015A are found to be similar for all three Reynolds numbers under zero degrees angle of attack. NACA 6409 airfoil has significantly different values under 0° of angle of attack when compared to other two NACA airfoils having positive lift coefficient values up to -6°. In addition, the highest lift/drag ratio was obtained for the NACA 6409 airfoil having a value of nearly 90. Comparing the FX series airfoils, the highest lift coefficient values were obtained for the FX 60-157 airfoil (Fig. 7). The lift to drag ratios were began to drop after 6° of angle of attack for FX 60-157 and FX 68-H-120 airfoils and for the FX 71-120 airfoil, it showed an increasing trend up to 10° of angle of attack. For 71-120, an accurate solution was not obtained because of simulation and convergence problems which could be related to occurrence of stall. Although a long solution time was given an adequate solution couldn't be obtained using CFD method and using a different turbulence model (k-ε realizable) ended with the same result.

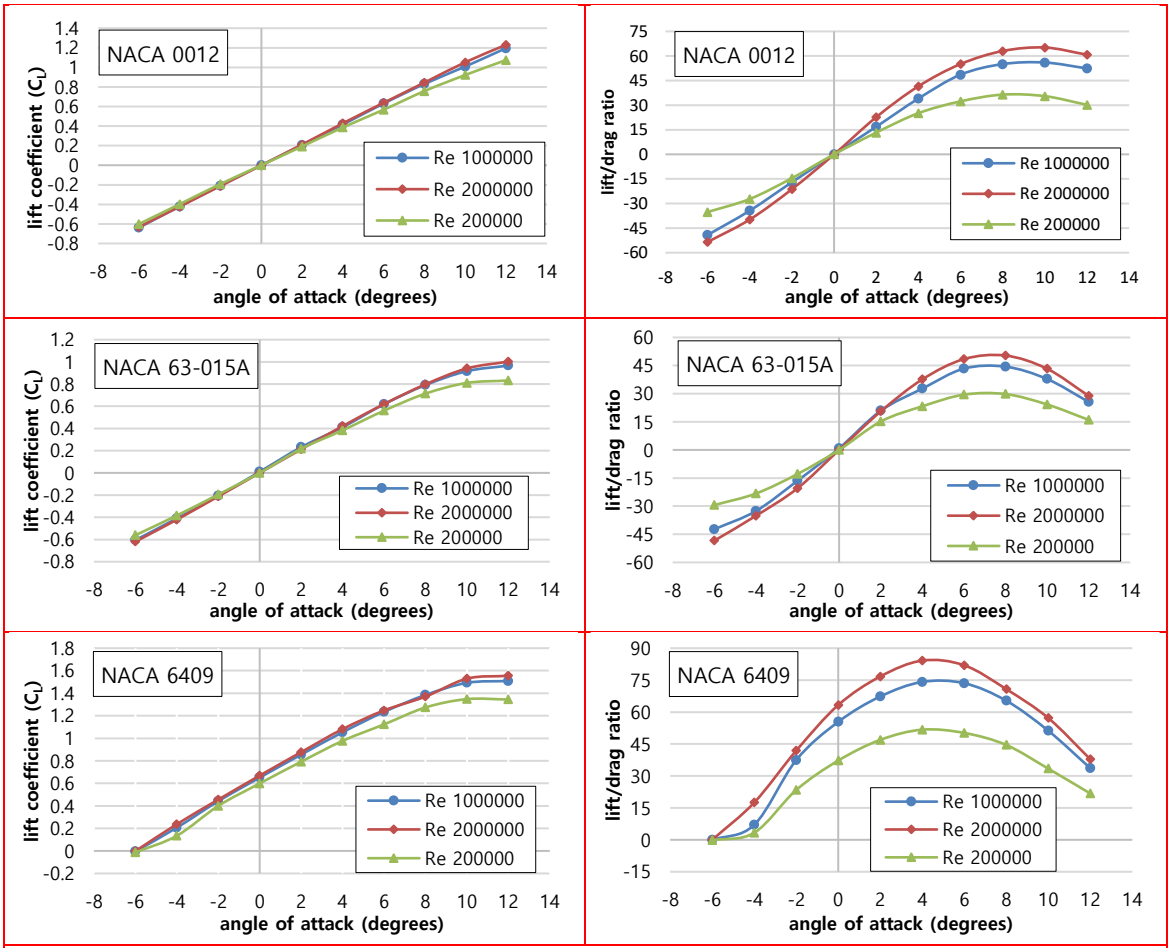

Fig. 6 Lift coefficients and lift/drag ratios of NACA 0012 (up), NACA 63-015A (middle) and NACA 6409 (down) airfoils

In Fig. 8, aerodynamic performances of the S series airfoils were compared. When comparing all three airfoils from the S family, the highest lift coefficient value was obtained for the S 4110 airfoil and lowest one for the S 806A airfoil. The lift coefficients at $Re = 2 \times 10^5$ for the S 4110 airfoil are found to be higher than the lift coefficients of the other two airfoils at Re $2x10^6$. S 1012 airfoil has showed similar performance to S 806A airfoil, however, slightly higher values were obtained for the S 1012 airfoil. For all S series airfoils, similar lift coefficients were obtained at $Re = 1 \times 10^6$ and $Re = 2 \times 10^6$, however, the values at $Re = 2 \times 10^5$ were slightly lower. The highest lift to drag ratio was obtained for the S 4110 airfoil at the angle of attack of 6° with the value of nearly 80. The lift to drag ratio has showed an increasing trend up to 8° of angle of attack for the S 1012 airfoil while the other two showed increasing trend up to 6°.

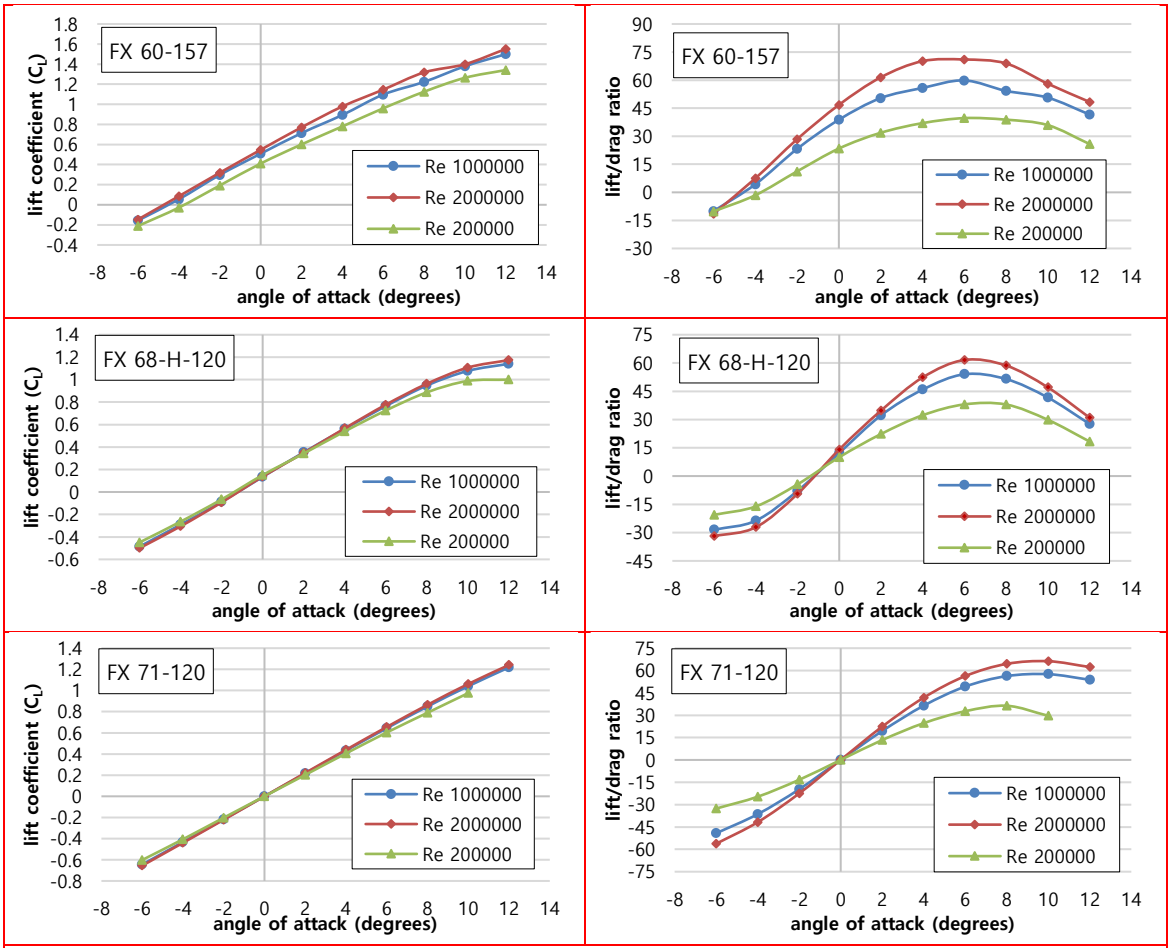

Fig. 7 Lift coefficients and lift/drag ratios of FX 60-157 (up), FX 68-H-120 (middle) and FX 71-120 (down) airfoils

In Fig. 9, all airfoils were compared in terms of lift coefficient and lift to drag ratios at Re=1x10^6. According to the results, the lift coefficients of NACA 6409, S 4110 and FX 60-157 were found to be the highest ones. NACA 63-015A was the one with the lowest lift coefficient value. At 12° of angle of attack, all airfoils have lift coefficient values between 1-1.2 lift except the three highest lift creating airfoils. Till 6° angle of attack, highest lift/drag ratio was obtained from NACA 6409 airfoil, after 6° angle of attack, higher ratios were obtained for the S 4110 airfoil. At 12° angle of attack, the highest ratio was obtained for the FX 71-120 airfoil. Velocity distributions around NACA 63-015A, FX 60-157 and S 806A are shown from -6° to 12° of angle of attack at Re=1x10^6 in Fig. 10.

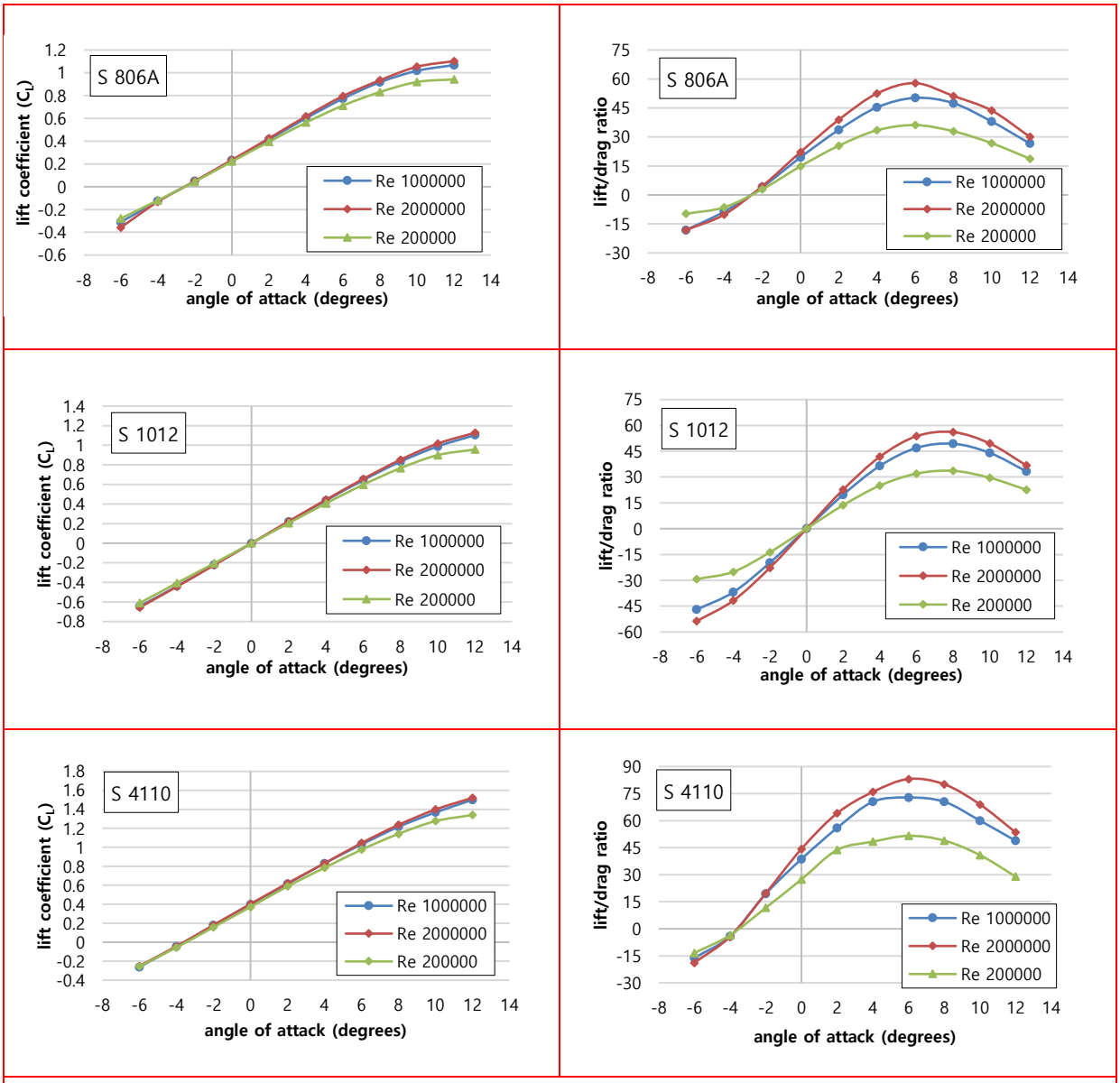

Fig. 8 Lift coefficients and lift/drag ratios of S 806A (up), S1012 (middle) and S 4110 (down) airfoils

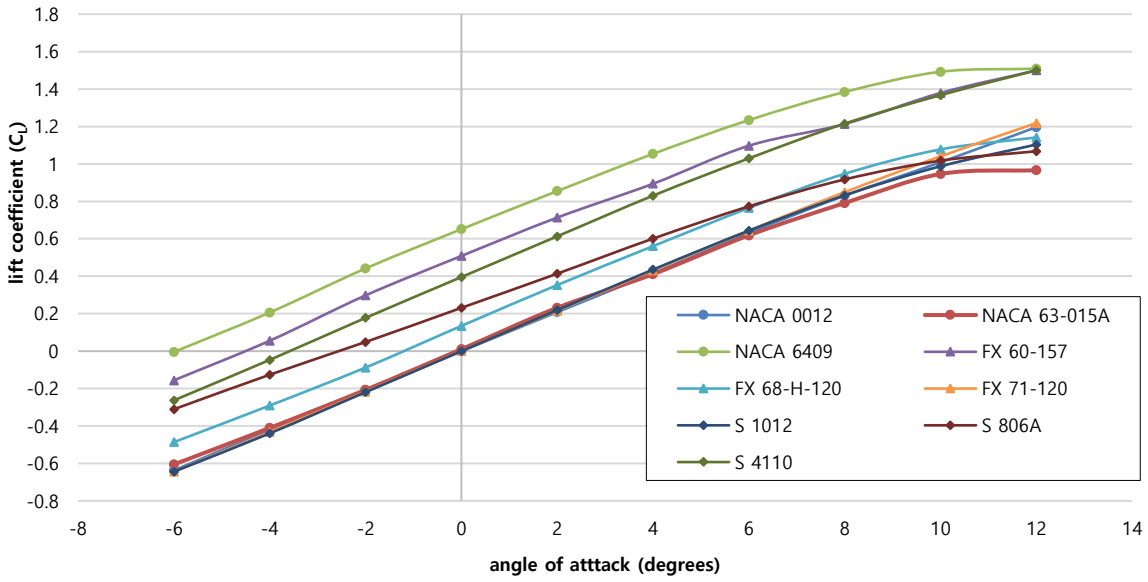

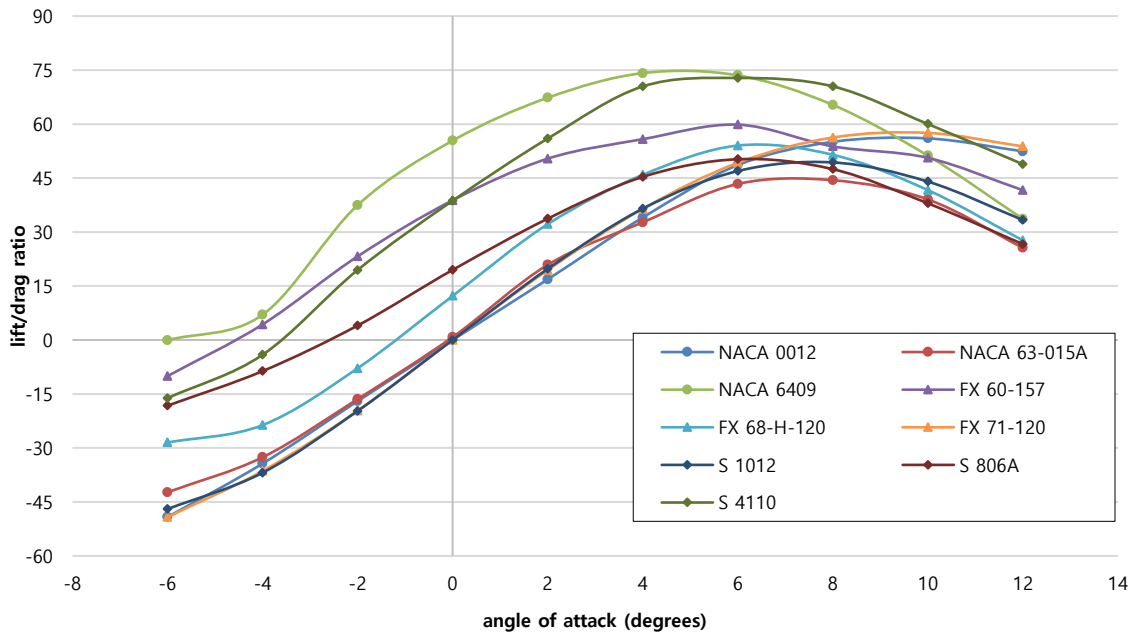

Fig. 9 Comparison of lift coefficients and lift/drag ratios at Re=10^6

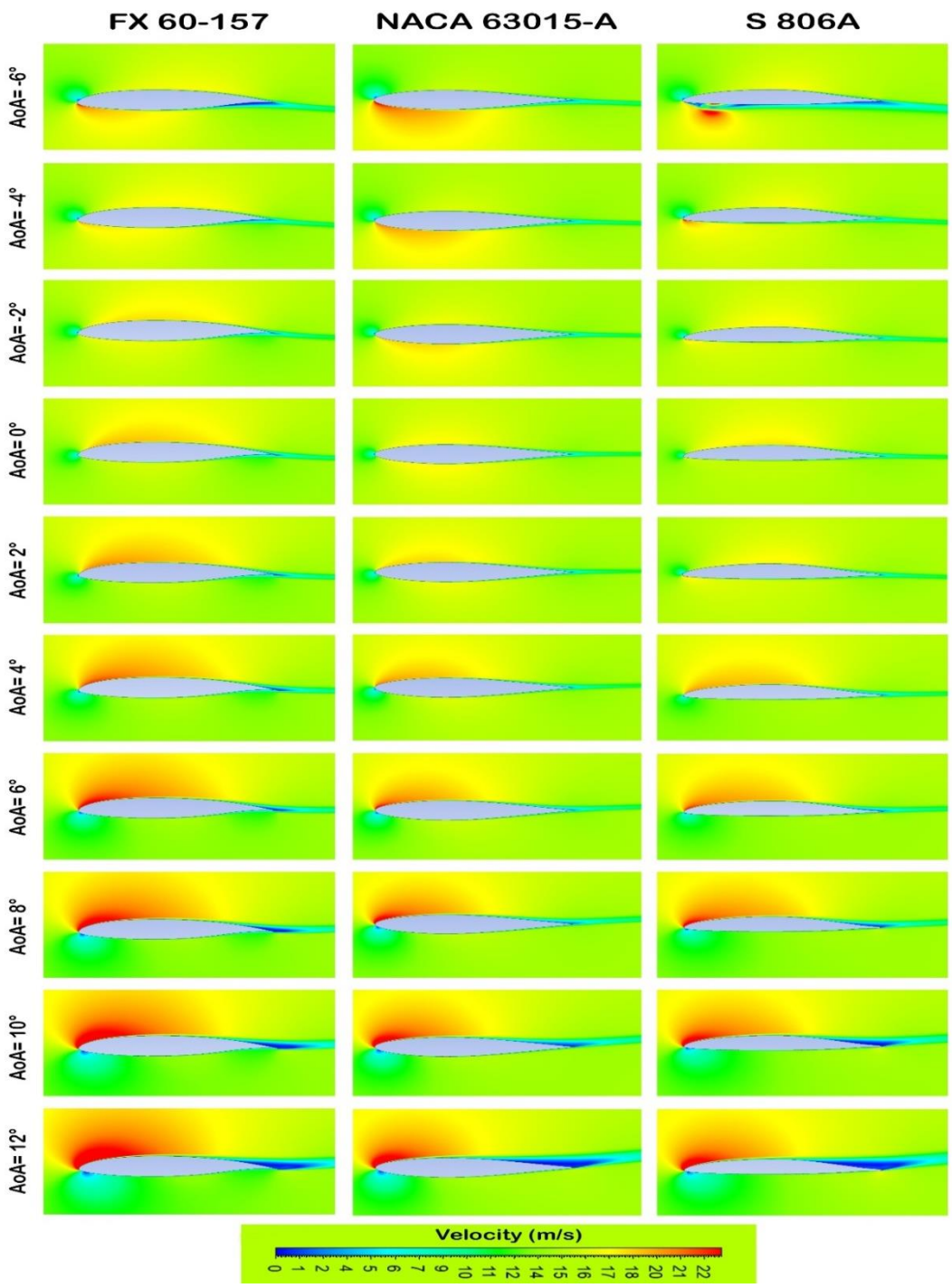

Fig. 10 Velocity contours of FX 60-157, NACA 63-015A and S806A airfoils at different angles of attack

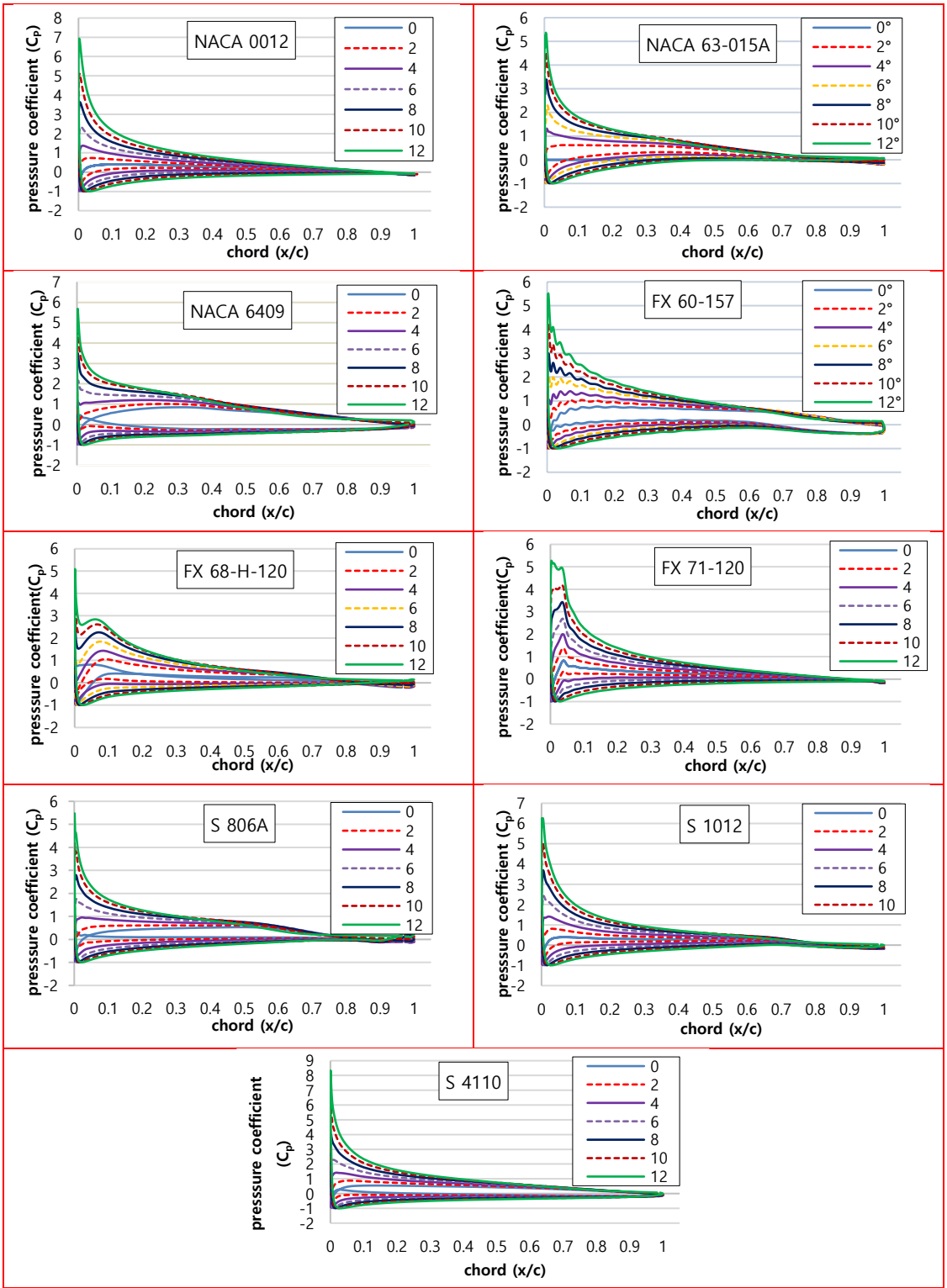

Fig. 11 Pressure distributions around the airfoils

The velocity contours of all three airfoils are showing similarities at higher angle of attacks. Maximum velocities at positive angle of attacks were obtained on the upper side of the airfoils near leading edges and minimum velocities were obtained at trailing edges as expected. For the angle of attacks between -2° and 2°, FX 60-157 and S 806A have higher velocities on the upper leading edge, where NACA 63-015A has maximum velocity on the lower leading edge. The location of the flow separation is moving towards the leading edge with the increase in angle of attack. For higher angle of attacks, the flow around NACA 63-015A and S 806 were separated earlier than FX 60-157. Moreover, a laminar separation bubble was occurred on the lower leading edge of the S 806A at -6° of angle of attack. Maximum velocities were obtained at highest angle of attacks for all airfoils. Pressure distribution around airfoils in terms of pressure coefficients at Re $1x10^6$ are presented for each airfoil at angles of attack between 0°-12° in Fig. 11. The pressure coefficients decrease rapidly from the leading edge to the trailing edge on the upper side, on the other hand, it increases slightly on the lower edge. Because of the geometric shape of the airfoils, there are irregularities on the leading edge. On the airfoils FX 68-H-120 and FX 71-120, there is a flow separation near the leading edge. The flow reattaches after a moment at the upper front of the leading edge. The pressure difference between upper and lower surfaces increases by increasing the angle of attack. For 12° angle of attack, the pressure coefficient of S 4110 reaches the highest value, when compared to the rest of the airfoils. Pressure difference increase with increasing airfoil thickness when comparing upper and lower surface. As expected, the more the pressure difference between upper and lower sides of the airfoils, the higher is the lift coefficient (Kaya *et al.* 2018) Increase of airfoil thickness also results in an increase of drag coefficient.

4. Conclusion

In this study, aerodynamic performances of nine airfoils from three different families were investigated by using CFD method. Firstly, CFD solution results of the NACA 0012 airfoil were compared with the available experimental data and it was found that numerically-simulated curves are in a good agreement with experimentally-obtained values. Especially, lift coefficients obtained from the CFD simulations are found to be very similar compared to experimental data. According to the flow simulation results, lift coefficients are generally increasing with increasing the angle of attack, however, lift to drag ratios are increasing only up to a specific angle of attack for all airfoils. When selecting an airfoil, those lift to drag ratios curves have to be analyzed well since it is highly related to the angle of attack and reynolds number. In the current study, lift to drag ratios reached maximum values between 6° and 8° of angle of attack for all the studied airfoils excluding FX 71-120 and NACA 6409. For the FX 71-120, airfoil stall has occurred after 10° at Re=$1x10^6$. A whirl occurred on the pressure side of the S 806A airfoil at -6° of angle of attack and this caused to a reduction in the aerodynamic performance of this airfoil at the mentioned angle of attack. With increasing Reynolds Number, all related coefficients have also increased. It is obtained that symmetric airfoils create nearly similar lift coefficients reaching their maximum values at similar angles of attack. Among the studied airfoils, maximum lift coefficients were obtained for FX 60-157 and S 4110 airfoils having lift coefficient values around 1.5 at Re=$1x10^6$ and 12 degrees of angle of attack.

References

Abinav, R., Nair, N.R., Sravan, P., Kumar, P. and Nagaraja, S.R. (2016), "CFD Analysis of Co Flow Jet Airfoil", *Indian J. Sci. Technol.*, **9**, 45. https://doi.org/10.17485/ijst/2016/v9i45/104686.

Abbott, I. H. and von Doenhoff, A. E. (1959), *Theory of Wing Sections*, Dover Publications, New York.

Alonso-Estebanez, A., del Coz Diaz, J. J., Rabanal, F. P. . lvarez, Pascual-Munoz, P. and Nieto, P. J. G. (2018), "Numerical investigation of truck aerodynamics on several classes of infrastructures ", *Wind Struct*., **26**(1), 35–43. https://doi.org/10.12989/WAS.2018.26.1.035.

Anitha, D., Shamili, G.K., Kumar, P.R. and Vihar, R.S., 2018. "Air foil shape optimization using CFD and parametrization methods", *Mater. Today: Proc*., **5**(2), 5364-5373. https://doi.org/10.1016/j.matpr.2017.12.122.

ANSYS Inc (2017), "ANSYS Fluent 18.0 Theory Guide", Ansys.

Aranake, A.C., Lakshminarayan, V.K. and Duraisamy, K. (2015), "Computational analysis of shrouded wind turbine configurations using a 3-dimensional RANS solver", *Renew. Energy*, **75**, 818-832. https://doi.org/10.1016/j.renene.2014.10.049.

Argyropoulos, C.D. and Markatos, N.C. (2015), "Recent advances on the numerical modelling of turbulent flows", Appl. Math. Model., **39**(2), 693-732. https://doi.org/10.1016/j.apm.2014.07.001.

Bansal, L., Chauhan, S., Kumar, C., Muzakkir, S.M. and Jafri, H.Z. (2017), "CFD Analysis of an Aerofoil Placed in Uniform Flow", *Int. J. Sci. Eng. Res*, **8**(7), 163-165.

Basta, E., Ghommem, M., Romdhane, L. and Abdelkefi, A. (2020), "Modeling and experimental co mparative analysis on the performance of small-scale wind turbines", *Wind Struct.*, **30**(3), 261-273. http://dx.doi.org/10.12989/was.2020.30.3.261.

Cakmakcioglu, S. C., Sert, I. O., Tugluk, O. and Sezer-Uzol, N. (2014), "2-D and 3-D CFD investigation of NREL S826 airfoil at low Reynolds numbers", *J. Phys. Conf. Ser.,* **524**(1), IOP Publishing.

Celik, Y., Ma, L., Ingham, D. and Pourkashanian, M. (2020), "Aerodynamic investigation of the start-up process of H-type vertical axis wind turbines using CFD", *J. Wind. Eng. Ind. Aerodyn.*, **204**, 104252. https://doi.org/10.1016/j.jweia.2020.104252.

Eggert, C.A. and Rumsey, C.L. (2017), "CFD study of NACA 0018 airfoil with flow control", NASA/TM–2017–219602.

Elsakka, M. M., Ingham, D. B., Ma, L., and Pourkashanian, M., (2018), "Effects of Turbulence Modelling on the Predictions of the Pressure Distribution around the Wing of a Small Scale Vertical Axis Wind Turbine", *7th European Conference on Computational Fluid Dynamics (ECFD 7)*, Glasgow, UK.

Gresho, P.M., (1991), "Some current CFD issues relevant to the incompressible Navier-Stokes equations", *Comput. Methods Appl. Mech. Eng.,* **87**(2-3), 201-252. https://doi.org/10.1016/0045-7825(91)90006-R.

Ilhan, A., Bilgili, M., and Sahin, B. (2018), "Analysis of aerodynamic characteristics of 2 MW hori zontal axis large wind turbine", *Wind Struct.*, **27**(3), 187-197. http://dx.doi.org/10.12989/was.2018.27.3.187

Kapsalis, P.C.S., Voutsinas, S. and Vlachos, N.S., (2016), "Comparing the effect of three transition models on the CFD predictions of a NACA0012 airfoil aerodynamics", *J. Wind. Eng. Ind. Aerodyn*., **157**, 158-170. https://doi.org/10.1016/j.jweia.2016.07.007.

Kaya, M. N., Kose, F., Ingham, D., Ma, L. and Pourkashanian, M. (2018), "Aerodynamic performance of a horizontal axis wind turbine with forward and backward swept blades", *J. Wind. Eng. Ind. Aerodyn*., **176**, 166-173. https://doi.org/10.1016/j.jweia.2018.03.023.

Kose, F. and Kaya, M. N. (2018), "Wind-Hydro Pumped Storage Power Stations to Meet the Energy Demands of Irrigation: Feasibility, Optimal Design and Simulation of a System," *J. Chin. Soc. Mech. Eng.*, **39**(2), 223-232. http://dx.doi.org/10.29979/JCSME.

Li, X., Zhang, L., Song, J., Bian, F. and Yang, K. (2020), "Airfoil design for large horizontal axis wind turbines in low wind speed regions", *Renew. Energy*, **145**, 2345-2357. https://doi.org/10.1016/j.renene.2019.07.163.

Lin, Y. T., and Chiu, P. H. (2020), "Influence of leading-edge protuberances of fx63 airfoil for horizontal-axis wind turbine on power performance", *Sustain. Energy Technol. Assess.*, **38**, 100675.

https://doi.org/10.1016/j.seta.2020.100675.
Manwell, J.F., McGowan, J.G. and Rogers, A.L. (2010), *Wind energy explained: theory, design and application*, John Wiley & Sons.
Matyushenko, A. A., Kotov, E. V. and Garbaruk, A. V. (2017), "Calculations of flow around airfoils using two-dimensional RANS: an analysis of the reduction in accuracy", *St. Petersburg Polytech. Univ. J.: Phys Math*., **3**(1), 15-21. https://doi.org/10.1016/j.spjpm.2017.03.004.
Menter F.R. (1992), "Influence of freestream values on k–omega turbulence model predictions", AIAA J. **30**, 1657–1659. http://dx.doi.org/10.2514/3.11115.
Menter F.R. (1994), "Two-equation eddy-viscosity turbulence models for engineering applications", AIAA J. **32**, 1598–1605. http://dx.doi.org/10.2514/3.12149.
Morgado, J., Vizinho, R., Silvestre, M.A.R. and Páscoa, J.C. (2016), "XFOIL vs CFD performance predictions for high lift low Reynolds number airfoils", *Aerosp. Sci. Technol.*, **52**, 207-214. https://doi.org/10.1016/j.ast.2016.02.031.
Patel, K. S., Patel, S. B., Patel, U. B., and Ahuja, A. P. (2014), "CFD Analysis of an Aerofoil", *Int. J. Eng. Res.,* **3**(3), 154-158.
Rostami, M.V., Saghafian, M., Sedaghat, A. and Miansari, M. (2011), "Numerical investigation of turbulent flow over a stationary and oscillatory NACA0012 airfoil using overset grids method'', Int. *J. Numer. Methods Fluids*, **67**, 135-154. https://doi.org/10.1002/fld.2332.
Shantanu S.Bhat, Raghuraman and N.Govardhan (2013), ''Stall flutter of NACA 0012 airfoil at low Reynolds numbers'', *J. Fluids Struct.*, **41**, 166-174. https://doi.org/10.1016/j.jfluidstructs.2013.04.001.
Siauw, W. L., Bonnet, J.P., Tensi, J., Cordier L., Noack B. R. and Cattafesta L. (2010), "Transient Dynamics of the flow around a NACA 0015 airfoil using fluidic vortex generators," *Int. J. Heat Fluid Flow*, **31**(3), 450-459. https://doi.org/10.1016/j.ijheatfluidflow.2010.02.028.
Spurthy, S., Sumukha, G.D., Prathik, B.V., Naveen, R., Srikanth, H.V. and Sridhar, K., (2016), "Study on effect of surface modification on aerodynamic characteristics of Eppler 387 airfoil", *AIP Conf. Proc*., **2204(**1), AIP Publishing LLC. https://doi.org/10.1063/1.5141573.
Sreejith B.K., Sathyabhama A. (2018), ''Numerical study on effect of boundary layer trips on aerodynamic performance of E216 airfoil'', *Eng. Sci. Technol. an Int. J.*, **21**, 77-88. https://doi.org/10.1016/j.jestch.2018.02.005.
Srinath, D.N. and Mittal, S. (2009), "Optimal airfoil shapes for low Reynolds number flows", *Int. J. N umer. Methods Fluids,* **61**(4), 355-381. https://doi.org/10.1002/fld.1960.
Tarhan, C. and Yilmaz, I. (2019), "Numerical and experimental investigations of 14 different small wind turbine airfoils for 3 different reynolds number conditions", *Wind Struct.*, **28**(3), 141–153. https://doi.org/10.12989/was.2019.28.3.141.
Tasci, M. O., Karasu, I., Sahin, B. and Akilli, H. (2020), "Investigation of crossflow features of a slender delta wing", *Wind Struct.*, **31**(3), 229-240. http://dx.doi.org/10.12989/was.2020.31.3.229.
Troolin, D. R., Longmire, E. K. and W. T. Lai (2006), "Time resolved PIV analysis of flow over a NACA 0015 airfoil with Gurney flap," Exp. Fluids, **41**, https://doi.org/10.1007/s00348-006-0143-8.
Tu, J., Yeoh, G.H. and Liu, C. (2018), *Computational fluid dynamics: a practical approach*, Butterworth-Heinemann.
Younsi, A., zamree bin abd Rahim, S. and Rezoug, T. (2019). Aerodynamic investigation of an airfoil under two hovering modes considering ground effect. *J. Fluids Struct*., **91**, 102759. https://doi.org/10.1016/j.jfluidstructs.2019.102759.
Zamani, M., Maghrebi, M.J. and Moshizi, S.A. (2016), "Numerical study of airfoil thickness effects on the performance of J-shaped straight blade vertical axis wind turbine", *Wind Struct.*, **22**(5), 595–616. https://doi.org/10.12989/WAS.2016.22.5.595.